THE JOURNAL OF PHYSICAL CHEMISTRY B

ARTICLE

pubs.acs.org/JPCB

Color Tuning in Binding Pocket Models of the Chlamydomonas-Type Channelrhodopsins

Kai Welke,[†] Jan S. Frähmcke,[‡] Hiroshi C. Watanabe,[†,§] Peter Hegemann,[¶] and Marcus Elstner*[,†]

[†]Institute of Physical Chemistry, Karlsruhe Institute of Technology, Kaiserstrasse 12, 76131 Karlsruhe, Germany

[‡]Institute for Physical and Theoretical Chemistry, TU Braunschweig, Hans-Sommer-Strasse 10, 38160, Braunschweig, Germany

[§]Japan Society for the Promotion of Science, Ichiban-cho 8, Chiyoda-ku 102-8472 Tokyo, Japan

[¶]Institute of Biology, Humboldt-Universität zu Berlin, Invalidenstrasse 42, 10115 Berlin, Germany

Supporting Information

ABSTRACT: We examined the shift of absorption maxima between the chlamydomonas-type channelrhodopsins (ChRs) and bacteriorhodopsin (BR). Starting from the BR X-ray structure, we modeled the color tuning in the binding pockets of the ChRs by mutating up to 28 amino acids in the vicinity of the chromophore. By applying the efficient self-consistent charge density functional tight binding (SCC-DFTB) method in a quantum mechanical/molecular mechanical (QM/MM) framework, including explicit polarization and calculating excitation energies with the semiempirical OM2/MRCI method and the ab initio SORCI method, we have shown that multiple mutations in the binding pocket of BR causes large hypsochromic shifts that are of the same order as the experimentally observed shifts of the absorption maxima between BR and the ChRs. This study further demonstrates that mutations in the proximity of the Schiff base and complex counterion lead to a stronger but more flexible interaction with the retinal, which could serve as a possible explanation for the spectral patterns found in the ChRs.

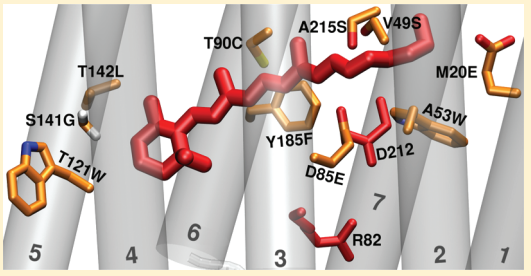

INTRODUCTION

The channelrhodopsins (ChRs) are a group of closely related seven-transmembrane proteins that uniquely combine the functions of a photoreceptor and ion channel in a single protein. Until now, five of them have been characterized: Channelrhodopsin-1 and -2 of *Chlamydomonas reinhardtii* (ChR1,[1] ChR2[2]), Volvox Channelrhodopsin-1 and -2 of *Volvox carteri* (VChR1, VChR2),[3−5] and recently Mesostigma Channelrhodopsin-1 of *Mesostigma viride* (MChR1),[6] the latter being less homologous to the first four than the first four among each other, hence the additional distinction of the four "chlamydomonas-type" channelrhodopsins.

Like their microbial relatives bacteriorhodopsin (BR), sensory rhodopsin II (sRII) or halorhodopsin, all-*trans* retinal serves as primary conformation of the chromophore in the dark-adapted state. Additionally, extraction experiments[7] and resonance Raman spectroscopic studies on ChR2[8] revealed the presence of significant amounts of 13-*cis* retinal as well, the ratio between all-*trans* and 13-*cis* being roughly 2:1. The retinal is covalently linked to the apoprotein via a protonated Schiff base linkage to a lysine residue in the seventh transmembrane helix. The isomerization of the retinal is accompanied by structural changes of the protein that have been confirmed by resonance Raman and IR spectroscopic studies.[8−10] The opening of the channel enables the influx of cations into the cell, which in turn leads to a change in membrane potential. In their native environment these potential changes are used to trigger a change of motion pattern of the organism in response to light (phototaxis and photophobic behavior). If expressed heterogeneously in a variety of cell types, the possibility of time- and space-controlled activation with light has led to the advancement of the field of optogenetics[11,12] and extended application of ChRs in neurosciences.

The absorption maximum (color) of the retinal can be tuned over a wide range of wavelengths by different protein environments. In light-adapted BR, the absorption maximum (λ_{max}) is at 568 nm (2.18 eV).[13] All ChRs are blue-shifted with respect to BR. Purified ChR1 shows a central λ_{max} at 463 nm (2.68 eV, pH 8)[14] for the dark-adapted state with a fine structure being visible in the spectrum. On acidification to pH 4.5, the λ_{max} is shifted to 505 nm (2.46 eV) and the fine structure has vanished. ChR2 does not exhibit such protochromism and shows identical UV/vis spectra under acidic and alkaline conditions. It shows two overlapping maxima at 450 nm (2.76 eV) and 470 nm (2.64 eV) with an additional shoulder at 413 nm (3 eV),[9] which already indicates the presence of multiple conformations in the ground state. The spectrum of VChR2 is nearly identical to ChR2 with two adjoining maxima at 445 and 475 nm and very little pH dependence.[5] Since other spectral and kinetic properties of VChR2 are not different from ChR2 and the sequence homology to ChR2 is very high, especially in the binding pocket region,[5] VChR2 will not be considered explicitly in this study. The spectrum of VChR1, however,

Received: September 5, 2011
Revised: November 10, 2011
Published: November 11, 2011

is different, being the most red-shifted protein of the known ChRs. At alkaline pH, VChR1 absorbs maximally at 500 nm (2.48 eV), while it is red-shifted to 540 nm (2.30 eV) at pH 6.[5] First action spectrum measurements of MChR1 revealed a maximum at 528 nm (2.35 eV, in HEK293 cells) at all probed pH values.[6] In this study, we focus on the discussion of the chlamydomonas-type channelrhodopsins ChR1, ChR2, and VChR1.

The understanding of the color tuning in these proteins may enable further understanding of the relationship between structure and function of the ChRs on a molecular level and generation of new ChR variants with desired spectral properties.[15] The biggest barrier so far is the lack of a crystal structure. While it is easily possible to generate three-dimensional models of the ChRs by the technique of homology modeling, this approach suffers from its own shortcomings. The sequences of the ChRs are very similar among each other, but the relation to other microbial rhodopsins is mainly restricted to helices 3 to 7. Major differences in helices 1 and 2 imply that the unique properties of the ChRs are connected to these helices. Finding a suitable template for homology modeling becomes a formidable challenge in the case of the ChRs. A subsequent study with focus on the structure of ChR1 and ChR2 starting from a reasonable sequence alignment is currently evaluated in our group.

As diverse as the rhodopsins are, so numerous are the studies on the color tuning in retinal proteins.[16−21] The λ_{max} is basically determined by the local retinal environment, while the color tuning results from three major effects: (i) the retinal configuration, (ii) the hydrogen-bonding interaction with the complex counterion, and (iii) the electrostatic interaction with the charged and polar residues of the protein environment. In most rhodopsins, mechanism (i), i.e., the retinal distortion, only plays a minor role,[16,17,22,23] although in the blue cone pigment, it seems to contribute more to the color tuning.[21,24] Mechanism (ii), the hypsochromic shift due to the negatively charged counterions, is a major factor in shifting the absorption of the retinal chromophore to lower wavelengths.[16,17,19,23,25] The effect of the counterions is partially balanced by a bathochromic shift of the binding pocket amino acids in some of the rhodopsins,[16,18,26] while only a few amino acids are able to shift the excitation energy by a significant amount.[16−18,26] The rest of the protein contributes to the color tuning to a lesser extent.[16]

Fortunately, it was shown that an understanding of a large portion of the color tuning may be achieved without knowledge of the complete structure. In the case of BR and sRII, 90% of the spectral shift between these two proteins (0.32 eV) arise from different neutral amino acids in their binding pockets and differences in the extended hydrogen-bonded network.[16] Based on this idea, it is the aim of this study (a) to generate binding pocket models based on the X-ray structure of BR and multiple mutations from a given sequence alignment, (b) to estimate the effects of single and multiple amino acid replacements on the excitation energy, and (c) to single out the major effects that contribute to the spectral tuning of these binding pocket models with respect to BR. If the binding pocket residues are indeed the major contribution to the color tuning, then much knowledge that is gained in studying the binding pocket models may be transferred to the full protein once a model has been made available.

In contrast to sRII and BR, which have very similar amino acid sequences, several glutamates are introduced into the N-terminal region of the ChRs. The effect of these additional, possibly negatively charged residues on the color tuning will be assessed in this work. It can be expected that these residues are involved in the channeling mechanism of the ChRs, making them undesirable targets for mutations, since it would significantly affect the channeling efficiency.

The computational strategy used in this work consists of QM/MM ground-state optimization and calculation of excitation energies with SORCI and OM2/MRCI, which was tested extensively[27] and applied successfully in studies of the spectral tuning in BR and sRII,[16] bovine rhodopsin,[28] and is currently also applied to binding pocket models of the blue cone visual pigment.

METHODS

General QM/MM Setup. The coordinates of the heavy atoms of BR were obtained from the X-ray structure of Luecke et al.[29] (PDB code 1C3W). Hydrogen atoms were added using the HBUILD module of the CHARMM program package.[30] Standard protonation states for titrable residues were assumed, except for D96, D115, and E204, which were modeled in their protonated form.[31,32] Harmonic restraints were imposed on all C_α atoms of the backbone and oxygen atoms of the water molecules that are farther than 12 Å away from the Schiff base. The screening effect of bulk solvent on charged amino acids was included based on the charge scaling scheme proposed by Dinner et al.[33] The partial charges of any charged solvent-exposed side chain are scaled down by a factor that is determined from solutions of the Poisson−Boltzmann equation.

For geometry optimization and molecular dynamics (MD) simulation, a hybrid quantum mechanics/molecular mechanics (QM/MM) scheme was used in form of the SCC-DFTB/CHARMM[34] implementation, which has been documented widely elsewhere.[35,36]

The QM method of choice is the approximate SCC-DFTB[37] method, which is about three orders of magnitude faster than full DFT methods, while describing the ground-state properties of the chromophore with comparable accuracy (bond lengths along the polyene chain, torsional barriers, etc.).[38] The remainder of the protein is described by the CHARMM27[39] force field. In this work, SCC-DFTB with (diagonal) third-order terms in charge density fluctuations was used, as described by Yang et al.[40]

Two different QM fragments were defined. A small QM region (labeled QM1), which consists of the retinal and the corresponding lysine side chain (K216 in BR) (1 residue, 63 atoms, +1 charge). A larger QM region (named QM6) also includes the counterions (D85, D212 in BR) and 3 resolved water molecules (W401, W402, W406 in 1C3W) (6 residues, 89 atoms, −1 charge).

The QM/MM boundary was chosen to be between the C_α and C_β atoms of the respective QM residues. The valence of the QM fragment was saturated with a hydrogen link atom, while the electrostatic interactions across the QM/MM boundary were treated by the "divided frontier" scheme.[41]

To test the stability of the binding pocket models, short QM/MM MD simulations were performed with SCC-DFTB/CHARMM with a time step of 1 fs. After heating to 300 K and equilibration, the Nosé−Hoover thermostat[42,43] was applied.

Vertical excitation energies for the transition between the S_0 and S_1 state of the retinal (ΔE_{S1-S0}) were calculated on two different levels. First, the efficient semiempirical OM2/MRCI[44,45] method as implemented in the MNDO99 program package[46] was applied. It was shown[16,27] that the OM2/MRCI excitation energy overestimates values obtained with more accurate ab initio

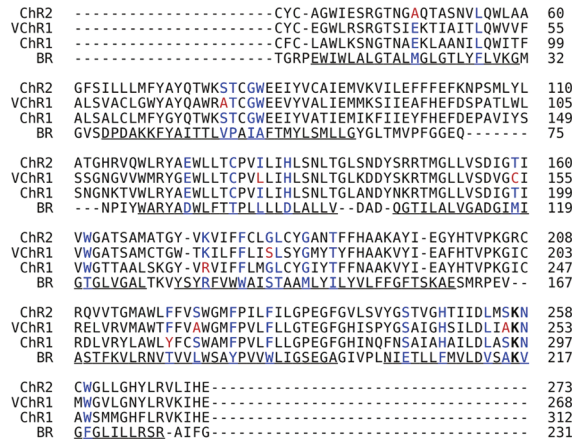

Figure 1. Sequence alignment:[2,4] blue = mutations for the binding pocket models, red = differences between ChRs, underlined = helices of BR.

methods, but that differences between various proteins are described well.

As an ab initio method to calculate excitation energies, the SORCI method was applied[47] (spectroscopy oriented CI) as implemented in the ORCA program package.[48] The various thresholds of the SORCI method were set in accordance with previous studies.[16,27] Excitation energies obtained with SORCI agree well with those of CASPT2.[27] The SV(P) basis set[49] was used with diffuse s- and p-functions on carboxylate oxygen atoms of anionic residues.[50]

To improve the electrostatic representation of the protein, we replaced the CHARMM27 point charges by the explicitly polarized polar.h model, which was benchmarked for peptides and applied to various retinal proteins.[28,51−53] This model combines polarization-free point charges with an induced atomic dipole model in response to the S_0 and S_1 charge distribution of the QM region.

Perturbation Analysis. A way to measure the impact of any amino acid on the excitation energy of the chromophore is by a perturbational approach, similar to Hayashi et al.[17] For a fixed protein geometry, each side chain is "mutated" into glycine, which effectively removes the charges of the side chain, but keeps the residue neutral. The electrostatic shift of residue I in a given protein is then defined as

$$\mathrm{ES}(I) = \Delta E(\text{wildtype}) - \Delta E(\text{w/o charges of } I) \quad (1)$$

describing the effect of the presence of the side chain of residue I on the vertical excitation energy. The electrostatic shift difference may then be defined as

$$\Delta\mathrm{ES} = \mathrm{ES}^{\mathrm{ChR}}(I) - \mathrm{ES}^{\mathrm{BR}}(I) \quad (2)$$

accounting for the different electrostatic effects of residue I between any ChR and BR.

Choosing the Binding Pocket Residues. The binding pocket models of the ChRs are based on the QM/MM-optimized structure of BR. Every amino acid that has at least one heavy atom within 6 Å of the retinal is defined to be part of the binding pocket. There are 34 amino acids within this distance, excluding the retinal binding site K216. Of these, 10 are conserved and 24 are different (Figure 1) between BR and ChR1/ChR2. Thirteen residues are conserved between BR and VChR1, reducing the number of mutations for the binding pocket model of VChR1.

Several alignments of BR with the ChRs are available,[2,54,55] each with its own advantages and disadvantages. For this work, an alignment published by Nagel et al.[2] (and Zhang et al.[4] for VChR1) was chosen with slight modifications: any gap inside of a presumptive helical region was moved to the nearest loop.

To include long-range electrostatic effects of charged and polar amino acids, a perturbation analysis as described above was performed. Those amino acids with $|\mathrm{ES}| \geq 0.01$ eV (eq 1) were also included in the binding pocket. For a complete list of mutations, see the Supporting Information.

Two histidines are introduced into the binding pocket region (D96H,[56] F208H), which were modeled neutral, since both D96 and F208 are neutral residues in BR. Another titrable residue is introduced into the binding pockets of ChR1 and VChR1 with the M20E mutation (helix 1). As mentioned above, the sequence homology of helices 1 and 2 of the ChRs to any microbial rhodopsin of known structure is very low, which makes a unique alignment difficult. Therefore, the mutations in helices 1 and 2 are highly dependent on the chosen alignment. In the alignment underlying this study,[2] M20 of BR is aligned to E87 of ChR1, which is involved in the pH-dependent color tuning of ChR1[57] (and by homology possibly VChR1, too), hence the protonation state may be pH-dependent. The glutamate was modeled as charged, corresponding to alkaline conditions.

In many cases, the mutated side chains can adopt multiple conformations (rotamers). Especially in the case of charged or polar amino acids, the different orientations may influence the excitation energy of the retinal. In any such case the most preferable conformation of the mutated side chain was taken. This was determined by (a) the stability in short QM/MM MD simulations and (b) lowest energy of the QM/MM optimized geometry, if (a) did not allow to distinguish between stable conformations.

The size of the mutated side chains often deviates from that of the original residues. Since proteins form rather compact units, voids are likely to be filled with water molecules. In this work, three additional water molecules were introduced into in the binding pocket in the vicinity of the Schiff base.

Homology Models of the Channelrhodopsins. The sequence of each ChR was aligned to the BR sequence according to Figure 1. For the ChR only the sequences of the presumptive transmembrane region was used, dismissing the large C-terminal ends. Homology modeling was performed with DeepView[58] and the SWISS-MODEL[59] web server with the binding pocket models as template structures. Standard protonation states were assumed on all titrable residues, except D195 (ChR1), D156 (ChR2), and D151 (VChR1), which are aligned to D115 in BR and confirmed to be protonated in ChR2.[60] The homology models were optimized with the same settings as described in the general QM/MM setup.

RESULTS AND DISCUSSION

Calibration of the Computational Model. We investigated the impact of different approaches to the computation of excitation energies in retinal proteins in previous studies.[27,51,52] The conclusions drawn from these studies are threefold. First, different QM methods applied for optimizing the retinal's geometry lead to very different values for the bond length alternation (BLA, difference between average single and double bond lengths), which leads to systematic shifts of excitation energies. In general, DFT methods within the generalized gradient approximation, subsuming the approximate SCC-DFTB here, underestimate the

BLA, overestimating the conjugation in the π-system of the retinal, which leads to bathochromic shifts of about 0.1 eV.[27] This can be considered a systematic offset of our methodology in all retinal proteins, i.e. we expect all modeled ChRs to be red-shifted by this amount.

Second, for the calculation of excitation energies, different QM methods lead to different values for the same geometry, implying that different methods capture the response of the QM region to the external electric field exerted by the protein environment differently. Third, additional bathochromic shifts of the excitation energies due to the polarization of the protein are found in the retinal proteins studied so far.[28,51−53]

On the basis of the results of Wanko et al.,[27] we chose the multireferential CI method SORCI for the calculation of excitation energies. This choice is justified by the nice agreement of calculated excitation energies to experimental absorption maxima of several rhodopsins.[28,52,53] By judging from the literature, SORCI and the CASPT2 method seem to be comparable in this aspect. To verify this choice in greater detail, a comparison of our results on BR with recent calculations using CASPT2 may prove beneficial.

Regarding the absorption of retinal in the gas phase, a recent analysis of Rajput et al.[61] showed maxima of 2.03 eV (610 nm) for the 6s-*trans*-all-*trans* configuration. CASPT2 excitation energies with CASSCF-optimized geometries agree well with these values (2.00 eV). In light-adapted bR, the retinal is in its 6s-*trans*-all-*trans* configuration, which we also adapted for the modeling in the ChRs. We find an excitation energy of 1.94 eV for a SCC-DFTB gas-phase optimized structure, which is indeed red-shifted by 0.1 eV with respect to the experimental value, due to the overemphasized delocalization in GGA-DFT as mentioned above.

The electric field exerted by the protein is thought to have a twofold influence on the chromophore: (a) a hypsochromic shift due to the interaction with the counterion(s) and (b) a shift due to the remaining binding pocket amino acids. These two values can easily be obtained by calculating the excitation energy of the retinal in the BR-optimized conformation in the presence of (a) only the charges of the counterions, or (b) all point charges of the protein.

A recent QM/MM calculation of Altoè et al.[26] obtained with CASPT2 on a CASSCF/AMBER-optimized geometry of BR yields an excitation energy of 2.32 eV, which is slightly blue-shifted with respect to the experimental λ_{max} of 2.18 eV, as expected due to the neglect of protein polarization. The shift with respect to the retinal (in the protein conformation, without protein point charges) was reported to be 0.3 eV. With SORCI, we find a BR excitation energy of 2.32 eV, and the shift with respect to retinal is 0.45 eV. There are multiple possible origins of this discrepancy. First, Altoè et al. use AMBER charges, while we employ CHARMM point charges in our calculation. Depending on the system, this may lead to differences of about 0.05 eV.[52] Second, we employ a charge-scaling procedure based on the solutions of the Poisson−Boltzmann equation for all charged residues that are assumed to be surrounded by bulk solvent. The effect of this is small but can attribute to shifts of up to 0.08 eV.[52] Third, the issue of different retinal geometries on the solvent shift has not been disclosed yet. It is possible that a retinal with smaller BLA, as used in our calculations, leads to a larger response to external electrical fields.

Note, however, that the polarizable charge model used in this work removes the first two effects in our calculation. Therefore, these factors only affect the comparison to CASPT2. The hypsochromic shift due to the presence of the counterions' point charges is reported as 0.87 eV in the CASPT2 calculations,[26] while with our setup we obtain a shift of 0.93 eV. The comparison of both values is again subject to the aforementioned differences (point charge models, solvation effect), albeit to a lesser extent than the full QM/MM values. The good agreement implies that both methods react similarly to the presence of point charges.

On the basis of this comparison, we expect SORCI and CASPT2 to be of comparable accuracy for the calculation of excitation energies in retinal proteins.

Table 1. Shifts of Excitation Energies of Selected Single Mutations[a] (Values in eV)

			QM1		QM6	
helix	mutation	protein	OM2/MRCI	SORCI	OM2/MRCI	SORCI
1	M20E	ChR1, VChR1	0.40	0.47	0.38	0.47
2	V49S	ChR1, ChR2	0.04	0.02	0.03	0.01
	A53W	all	−0.02	−0.07	−0.04	−0.09
3	D85E	all	0.06	0.02	0.06	−0.03
	T90C	all	0.10	0.04	0.10	−0.01
4	T121W	all	0.03	0.03	0.03	0.02
5	S141G	ChR1, ChR2	0.12	0.09	0.12	0.08
	T142L	all	0.03	0.00	0.03	0.03
6	Y185F	all	−0.03	−0.04	−0.03	−0.05
7	A215S	ChR1, ChR2	0.08	0.02	0.08	−0.04
sum of all 27 mutations in ChR1[b]			0.97	0.70	0.87	0.30
sum of all 28 mutations in ChR2			0.59	0.21	0.51	−0.17
sum of all 25 mutations in VChR1			0.71	0.46	0.63	0.21

[a] First letter and number refer to BR sequence; last letter designates corresponding amino acid of a ChR. [b] The number of mutations that is necessary to generate the binding pocket of the ChR from BR as described in the text.

Single Mutations from BR to ChR. As a first step, each amino acid in the binding pocket region is mutated individually to estimate its effect on the vertical excitation energy (Table 1; for a complete list of all single mutations, refer to the Supporting Information).

Upon excitation, positive charge is redistributed from the Schiff base toward the β-ionone ring of the retinal. Therefore, it can be expected that negative charges introduced in the vicinity of the Schiff base stabilize the S_0 state relative to the S_1 state, causing a hypsochromic shift. Likewise, a negative charge near the β-ionone ring should stabilize the S_1 state relative to the S_0 state, hence causing a bathochromic shift and vice versa.

The largest shift is therefore induced by the M20E mutation, which can be explained by its negative charge and position close to the protonated Schiff base (Figure 2). The magnitude of this shift alone is of the same order as the overall shift between BR and the ChRs. Due to its negative charge, it polarizes the surrounding amino acids to a high degree. Since MM point charges are not polarizable, this effect is neglected, leading to excitation energies that are too high. If the polar.h model is applied, the charge distribution of the protein is allowed to relax in response to the charge. Consequently, the shift caused by the M20E mutation is reduced to 0.2 eV.

As already established for the color tuning between BR and sRII,[16,17] the effects of the other amino acids are rather limited. The residues S141, T142 (near the β-ionone ring), and A215

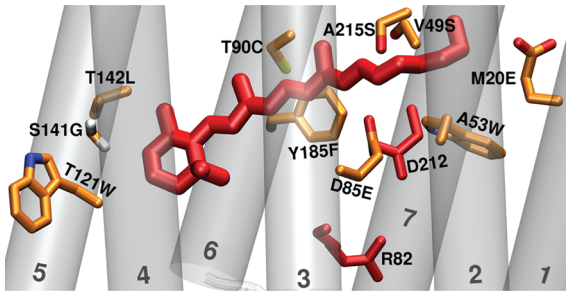

Figure 2. Positions of mutated amino acids in the binding pocket of ChR1: orange = mutations listed in Table 1, red = conserved residues D212 and R82, and the chromophore at K216.

(close to the protonated Schiff base of BR) have been shown to be significant for the color tuning. In the ChRs, their mutation also leads to shifts of the excitation energy of about the same size as mentioned in the previous study.[16] The positions of these amino acids in the binding pocket can be seen in Figure 2.

Generally, the induced shifts vary only slightly for different QM regions and methods. The semiempirical OM2/MRCI method agrees well with the ab initio SORCI method for small shifts. Upon summation of the single shifts for each protein, the differences between the methods are most pronounced, becoming as large as 0.7 eV (ChR2, QM6). The deviations can be traced back to mutations like M20E, D85E, T90C, and A215S, which are close to the Schiff base region of the retinal. In these cases, the shifts are accurately described only by the large QM6 region and the SORCI method. The effect of increasing the QM region is twofold. First, a transfer of a small fraction of charge is permitted between the chromophore and its counterions (about 0.1 e). Second, the counterions are allowed to be polarized by the chromophore and the surrounding (MM) amino acids. This different description of the electron density on the retinal and complex counterion also causes slight differences in the optimized structures. Combined, these three effects lead to differences between QM1 and QM6 excitation energies and shifts. Both the charge transfer and the polarization of the counterions are described differently on the OM2/MRCI and SORCI levels, resulting in different shifts of excitation energies.

Perturbation Analysis. To check for amino acids that are farther than 6 Å away from the retinal and influence its excitation energy, a perturbation analysis was performed. As described before, each residue is mutated into a glycine, which corresponds to deleting the charges of the side chain. The individual electrostatic shift (ES, eq 1) measures the effect of this specific residue on the excitation energy of the chromophore.

Eighteen residues have an ES larger than 0.01 eV (Figure 3), with 12 of them being within 6 Å of the Schiff base. Of those 6 amino acids that are farther away, 4 residues are different between BR and the ChRs, R82, and E194 being conserved in the ChRs. On the basis of this analysis, these 4 residues are incorporated into the binding pocket models. They are mutated rather conservatively (D96H, R134K, T78Y/F, E204S). Since D96 and E204 perform important functions during the proton-pumping photocycle of BR, their mutations indicate functional differences between BR and the ChRs. Indeed, the mutation of the histidine back to an aspartate (H173D in ChR1 numbering) leads to a complete loss of light-gated conductance.[1]

Mutation Induced Shifts of Vertical Excitation Energies of the Binding Pocket Models. The mutations selected due to the close distance to the retinal (24 in ChR1/ChR2, 21 in VChR1) combined with those found in the perturbation analysis (3 in ChR1, 4 in ChR2/VChR1) generate the binding pocket models of the ChRs. They have vertical excitation energies ΔE_{S1-S0} that are shifted with respect to BR. These shifts are evaluated as $\Delta\Delta E = \Delta E_{S1-S0}(\text{binding pocket}) - \Delta E_{S1-S0}(\text{BR})$.

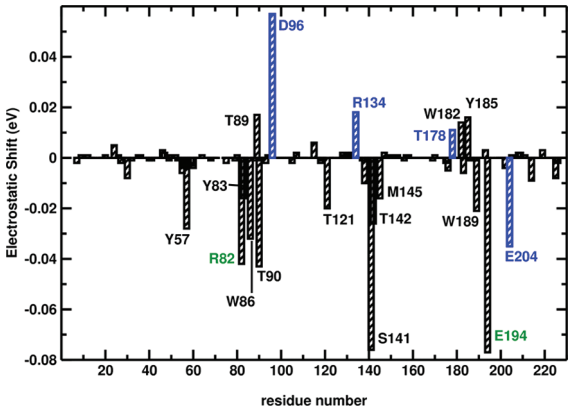

Figure 3. Perturbation analysis for BR (QM6; D85, D212 omitted): blue = residues farther than 6 Å away from the Schiff base *and* different between BR and ChRs, green = conserved R82 and E194, all other labeled residues are within 6 Å.

Table 2. Shifts of the Vertical Excitation Energies of the Binding Pocket Models with Respect to BR $\Delta\Delta E$ (in eV)

	method	ChR1	ChR2	VChR1
QM1	OM2/MRCI	0.51	0.28	0.40
	SORCI[a]	0.69	0.34	0.42
QM6	OM2/MRCI	0.61	0.38	0.40
	SORCI	0.74	0.46	0.38
exp		0.50	0.52	0.30

[a] With CHARMM point charges.

The binding pocket models are blue-shifted with respect to BR (Table 2), which is expected, considering the type (Figure 1) and location of the mutations (Figure 2). In ChR1, the 27 mutations lead to a hypsochromic shift of 0.74 eV (QM6 region, SORCI). This shift is 0.1 eV larger than the sum of the shifts from the single mutations (Table 1), indicating that the effects of mutations are not additive.

Instead of the M20E mutation in ChR1, the M20 is mutated into an alanine in ChR2, which is the main difference between these two binding pocket models. Therefore, the hypsochromic shift of ChR2 with respect to BR is smaller by 0.28 eV (QM6, SORCI), which is smaller than the M20E mutation alone (0.47 eV)—again showing the nonadditivity of the mutations. The M20E mutation is present in VChR1, but several other mutations that lead to hypsochromic shifts in ChR1 and ChR2 are absent (S141 and A215 are conserved, V49A is a conservative mutation). Thus, the hypsochromic shift for VChR1 is smallest of the three studied binding pocket models.

For small to medium (ChR2, VChR1) shifts, the OM2/MRCI and SORCI methods agree well. For ChR1, the shifts obtained with SORCI exceed the OM2/MRCI shifts by about 0.15 eV. As shown in Table 1, differences between the two methods occur mainly for mutations that are close to the chromophore and change the electrostatic environment considerably. The number

Table 3. Vertical Excitation Energies Obtained with Explicit Polarized Polar.h Model (SORCI/pol) Compared to SORCI/MM Values with CHARMM Point Charges (in eV)

	method	BR	ChR1	ChR2	VChR1
QM1	SORCI/MM	2.32	3.01	2.65	2.73
	SORCI/pol	2.17	2.64	2.50	2.58
QM6	SORCI/MM	2.40	3.14	2.86	2.78
	SORCI/pol	2.18	2.85	2.63	2.61
expt		2.18[13]	2.68[14]	2.70[a9]	2.48[5]

[a] The mean of both adjoining maxima 2.76 and 2.64 eV.

of such mutations is largest in ChR1, and therefore the difference between OM2/MRCI and SORCI is most pronounced.

Effect of Polarization on the Vertical Excitation Energies. Replacing the (fixed) MM point charges with the explicitly polarizable polar.h model leads to lower excitation energies (Table 3), 0.22 eV in the case of BR (QM6). The perfect agreement of the excitation energies with the experimental λ_{max} has to be assessed as a coincidence due to error cancellation. The SORCI method yields vertical excitation energies that are 0.05−0.1 eV below the experimental λ_{max} of gas-phase-optimized retinal.[27] In addition to the neglect of dispersion effects, it can be estimated that the polarization red-shifts the excitation energy too strongly.

In the ChRs the bathochromic shifts due to explicit polarization are similar to BR (ChR1 0.29 eV, ChR2 0.23 eV, VChR1 0.17 eV), which is surprising, considering how much the electrostatic environment of the chromophore is altered in the ChRs. This finding underlines the difficulty of estimating the effect of polarization a priori, which was also demonstrated in the case of the O-state of BR,[53] the last intermediate of the BR proton-pumping cycle: the excitation energy of the O-state is hardly lowered by explicit polarization, while the lowering is sizable for the BR ground state (Table 3), although both structures are similar. Thus, for the calculation of excitation energies, the inclusion of explicit polarization is vital, supporting the results of previous studies,[51−53] but shifts of excitation energies are hardly affected in this case.

Contribution of Different Retinal Geometries to the Overall Shift. The overall shifts (Table 2) result from several distinct contributions, which will be analyzed separately in the following. The first part to be analyzed is the different geometry of the retinal in BR on one hand and in the ChRs on the other. By calculating the excitation energies of the retinal in gas phase (QM1 without protein point charges), one can directly infer the shifts that result from different retinal geometries (Table 4). To rule out structural differences between QM1- and QM6-optimized structures, these excitation energies were calculated with the QM6-optimized structure. As stated above, our reference value for the unperturbed chromophore obtained with SORCI for the SCC-DFTB optimized 6s-*trans*-all-*trans*-retinal is 1.94 eV. This value agrees well with the experimental absorption maximum of the retinal at 2.03 eV.[61]

In the ChRs, the different retinal geometries lead to shifts of about 0.09 eV with respect to BR. This shift is slightly larger than between BR and sRII (0.05 eV).[16] Among the ChRs, the retinal geometry is similar, so that they also have similar excitation energies for the bare chromophore. One important parameter that correlates with the absorption maximum is the bond length alternation (BLA), defined as the averaged difference between single and double bond lengths. In the binding pocket models, the BLA increases,

Table 4. Excitation Energies (in eV) of the Chromophore (QM1 Region without External Point Charges, SORCI) and Structural Parameters of the Retinal (Distances in Å, Angles in deg)

	BR	ChR1	ChR2	VChR1
ΔE	1.87	1.96	1.95	1.96
planarity[a]	10.06	4.96	6.16	8.51
BLA[b] (in pm)	5.39	7.63	6.93	7.18
H-bond to[c]	W402	E85	E85	W402

[a] Average deviation of dihedral angles from planarity. [b] Bond length alternation = difference between averaged C−C single bonds and C═C double bonds. [c] Hydrogen bonding partner of the Schiff base.

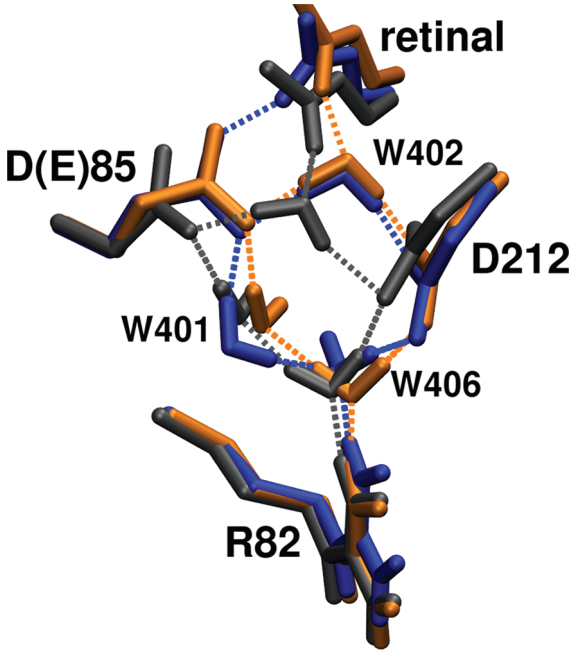

Figure 4. Different configurations of the hydrogen-bonded network of the retinal with its counterions in the binding pockets: BR = gray, ChR1/ChR2 = blue, VChR1 = orange.

as does the overall shift of the excitation energy. The shifts and structural parameters of the retinal (Table 4) indicate very similar geometries, implying that the different retinal geometries are just a small contribution to the large overall shift. This in turn implies that the BLA is not the reason for the large hypsochromic shift, but a consequence of the electrostatic interaction with the amino acids of the binding pocket. An increased BLA indicates a more pronounced double or single bond character. This can be seen in the increased planarity of the dihedral angles, especially around the formal C═C double bonds of the retinal backbone.

Visible structural differences are restricted to the β-ionone ring and a different conformation of the lysine side chain, which is connected to a different orientation of the N−H bond of the Schiff base (Figure 4).

Contribution of the Counterions to the Overall Shift. The complex counterion in BR is composed of D85, D212 and the three water molecules (W401, W402, W406 of 1C3W) between these residues. One of the counterions, D85, is replaced in all ChRs by a glutamate. The single mutation D85E induces only

Table 5. Excitation Energies of the Chromophore and the Protein and with Deleted Charges of the Counterions (in eV), Calculated with SORCI for the QM1 Region

	BR	ChR1	ChR2	VChR1
chromophore[a]	1.87	1.96	1.95	1.96
+HBN[b]	2.80	2.95	2.92	2.79
protein	2.32	3.01	2.65	2.73
−D(E)85	1.92	2.40	2.15	2.33
−D212	1.97	2.71	2.51	2.60
−CCI[c]	1.66	2.12	1.91	2.03
ES(CCI)[d]	0.66	0.89	0.75	0.70

[a] Same as Table 4. [b] Hydrogen-bonded network, QM1 in the presence of point charges of D(E)85, D212, R82, W401, W402, W406 only. [c] D85, D212, W401, W402, W406. [d] ES(CCI) = ΔE(protein) − ΔE(−CCI).

minor shifts of about 0.03 to 0.06 eV (Table 1) which is of the same order as the shift due to the different retinal geometry.

In BR, the two counterions impact the excitation energy to similar extent. The effects are not additive, since the replacement of both residues lead to a different shift than the sum of the single mutations.

Overall, the electrostatic shifts (ES, eq 1) of the complex counterion increases in all ChRs (Table 5). Compared to BR, the ΔES (eq 2) ranges from 0.06 eV in VChR1 to 0.25 eV in ChR1, with ChR2 being in the middle (0.11 eV). This correlates with the overall trend: the binding pocket models of VChR1 and ChR2 having similar shifts, and ChR1 being the most blue-shifted. By comparing the magnitude of the ΔES of the counterions (Table 5) with the overall hypsochromic shift (Table 2), it is shown that the increased interaction of the Schiff base with the counterions is a major contribution to the overall shift, although the effects are not additive.

If the charges of the counterions are removed (−CCI), the effect of the remaining amino acids are still included in the excitation energy value. In BR, the removal of the complex counterion leads to a bathochromic shift, which was also reported previously.[16,26] The excitation energies of the ChR binding pocket models without the counterions' charges are close to the gas-phase value of the retinal, suggesting that, in these models, the binding pocket residues do not cause a bathochromic shift. The hydrogen-bonded network causes a hypsochromic shift of about 0.9 eV in BR (see also ref 26), which is also found in ChR1 and ChR2, while this shift is smaller in VChR1.

The different ES of the two counterions in the ChRs are correlated to structural differences. On one hand, an increased distance between the retinal and the D212 leads to lower ES of this residue in the ChRs. On the other hand, a shorter distance between the retinal and E85 is accompanied by a higher ES. In VChR1, the distance between the retinal and the E85 is similar as in BR, suggesting a similar ES.

These different distances also correlate with different orientations of the N−H bond of the Schiff base (Figure 4). In BR, and VChR1, the N−H bond is oriented to a water molecule (W402 in BR X-ray structure 1C3W) resulting in similar ES of the counterions. In ChR1 and ChR2 on the other hand, the N−H bond is oriented toward one of the O_ε atoms of the E85 residue, leading to higher ES.

These data are assembled from QM/MM-optimized structures. During short QM/MM MD simulations the increased flexibility of the interaction of the Schiff base with its complex counterion becomes apparent. The hydrogen-bonding pattern of the BR starting structure seems to be conserved, albeit with increased flexibility of W401. While in BR the hydrogen bond between the Schiff base and W402 is highly conserved during the QM/MM MD, it switches from the E85 counterion to the water W402 back and forth. This switching of the interaction mode of the Schiff base in a more flexible binding pocket could be a hint toward the appearance of multiple absorption maxima in the spectra of the ChRs, as shown for ChR2 with two λ_{max} separated by 0.12 eV (20 nm).[9]

Table 6. Summed Differences of the Electrostatic Shifts for the Binding Pocket Models (QM6, OM2/MRCI, in eV)[a]

	ChR1	ChR2	VChR1
ΣΔES (all residues)	0.45	0.10	0.26
ΣΔES (binding pocket)[b]	0.44	0.13	0.23
ΣΔES (bp mutations)	0.48	0.23	0.27
ΣΔES (bp conserved)	−0.03	−0.10	−0.04

[a] Note that the summation excludes the counterions (E85 and D212). [b] 38 residues out of 227; 32 residues within 6 Å of the retinal (excluding both counterions) and 6 residues with large ES in the perturbation analysis in BR.

Contribution of the Binding Pocket Amino Acids. To analyze the contribution from the protein environment, a perturbation analysis is performed. By mutating each residue into a glycine, while keeping the geometry fixed, and subsequently calculating the excitation energy, one can extract the electrostatic effect of this residue. The perturbation analysis is evaluated in terms of the electrostatic shift difference, ΔES, as described before (eq 2).

The results of this analysis are shown in Table 6. The electrostatic shift differences between ChR1 and BR for all amino acids (excluding the counterions) sum up to 0.45 eV (ΣΔES all residues). This is almost identical to the summed shift of the binding pocket residues (ΣΔES binding pocket), indicating that the amino acids not in the binding pockets have the same ES as in BR, thus not contributing to the overall shift.

The major part of this shift is caused by the 27 mutations in the binding pocket (0.48 eV), while differences of the conserved residues (E194, D115, T89, R82, and Y57 with largest ΔES) cause a minor bathochromic shift of (−0.03 eV). This is due to a slightly different orientation of these residues in the binding pocket models compared to BR.

In ChR2, where the M20E mutation is replaced by M20A, the binding pocket mutations lead to a summed ΔES of 0.23 eV. Interestingly, the effect of conserved residues is larger than in the other ChRs, causing a bathochromic shift of −0.1 eV. The majority of this shift can be traced back to Y57, D115, and E194. Although the coordinates of these residues are nearly identical in the binding pocket models of ChR1 and ChR2, their effect on the excitation energy of the chromophore is different.

VChR1 again is similar to ChR1. As mentioned before, several mutations are missing (L93, S141, A215 are conserved) or conservative (V49A, L181A), so that the hypsochromic shift due to the mutations in the binding pocket is only 0.27 eV. The effect of the conserved binding pocket residues is similar to ChR1.

Estimate of the Contribution of the Rest of the Proteins—Evaluation of Homology Models. By mutating a limited amount of amino acids in the surrounding of the retinal, the binding pockets

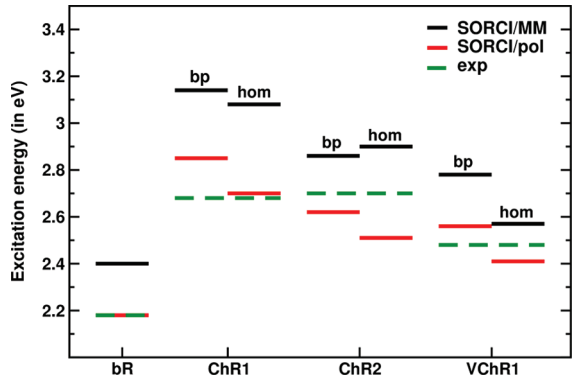

Figure 5. Comparison of vertical excitation energies of the homology models with binding pocket models.

of the ChRs can be modeled and their effect on the absorption properties of the chromophore can be estimated as described above. By using these binding pocket models as templates for homology modeling, the (electrostatic) effect of the rest of the protein can be estimated. These estimations have to be interpreted carefully, however, since the overall structure of the homology models is still very BR-like. In this manner, the effect of changing the protein around the binding pockets can be extracted.

It is shown in Figure 5 that the excitation energies of the homology models of ChR1 and ChR2 are similar to those obtained for the binding pocket models (Table 3), thus leading to hypsochromic shifts of similar magnitude. For VChR1, the excitation energy (QM6) is 0.2 eV lower than for the binding pocket model. The reason for this deviation is a larger structural rearrangement during the QM/MM optimization of the VChR1 homology model. For the homology models of ChR1 and ChR2, these rearrangements are smaller, resulting in similar excitation energies as for the binding pocket models.

According to the sequences of the ChRs, several charged residues are introduced into the N-terminal regions. The exact location of these charged residues highly depends on the sequence alignment, which makes an exact determination of their contribution to the color tuning in the ChRs difficult. In this particular alignment (Figure 1), several of the additional charged residues appear in the loop between helices 2 and 3, rendering them solvent exposed and thus screening their charges. Those amino acids that are in the helical region face into the membrane region or appear paired with oppositely charged residues thus nullifying their effect on the retinal. For this alignment, only two glutamates (ChR1: E122, E123; ChR2: E41; VChR1: E77, E78), but up to four positively charged residues (K80, K88, K115, K132; ChR2: K76, K93; VChR1: K44, R71, K88) are introduced in helix 2. The summed ES of these residues is smaller than 0.01 eV, meaning that for this alignment, the additional charged residues do not contribute significantly to the color tuning. However, the appearance of more positively than negatively charged residues is questionable for a cation-conducting channel.

■ CONCLUSIONS

To further expand their optogenetic toolbox, neuroscientists have created a demand for modified ChR variants. Color-shifted ChRs are desirable for multiple reasons: for in vivo applications, a ChR with an absorption maximum shifted to higher wavelengths (>520 nm) would significantly reduce scattering losses.[15] Moreover, ChRs absorbing light of different wavelengths allow for combinatory experiments that selectively activate different cell types with lasers of different wavelengths. The aim of our study was to achieve an understanding of the active sites of the ChRs and enable the search for possible targets for mutations that shift the λ_{max}, although our results show that multiple mutations have to be introduced to get a sufficient shift of the λ_{max}.

Several possibly negatively charged glutamates appear in the N-terminal region of the ChRs. While they may seem promising candidates for mutations that lead to bathochromic shifts, it is likely that they are involved in the cation-channeling function, thus making them undesirable targets. We showed the sequence dependence of the color tuning and, thus, the limits of the approach, since there is no unique alignment to known microbial rhodopsins for these glutamates. Their location in the protein—helix or loop—and hence their influence on the color tuning is highly dependent on the sequence alignment to the chosen template protein. In the specific alignment underlying our studies, the additional charged residues do not cause any significant excitation energy shift; instead, differences in the binding pocket are responsible for a large portion of the shift, as shown in Table 6.

Recently, it has been proposed that the major role of the electrostatic interaction with the binding pocket residues is to counterbalance the hypsochromic shift of the counterions, named "counterion quenching" by Tomasello et al.[18] The binding pocket residues have to have an overall bathochromic shift for the ultrafast photoisomerization of the retinal to occur. Since all rhodopsins contain the same cofactor and the counterions seem to shift the excitation energy to similar extents,[18,26] the counterion quenching suggests that the limits of (electrostatic) spectral tuning have to be overcome by the twisting of the retinal in strongly blue-shifted rhodopsin variants.

In our analysis of the ChR binding pocket models, however, we find only a slightly twisted retinal, the excitation energy of the isolated chromophore being only slightly shifted by 0.1 eV compared to BR, as shown in Table 4. On the other hand, we find no large bathochromic shift of the binding pocket residues in these models (Table 5). As discussed above, we expect the effects of the binding pocket on the excitation energy being described to similar extent by the CASPT2/CASSCF and SORCI/SCC-DFTB approaches. On a qualitative level, one can also compare the sequences of the ChRs to BR. Although a unique sequence alignment is not available at this moment, several amino acids in regions that are similar in different alignments,[2,54,55] i.e., helices 3 to 7, lead to hypsochromic shifts as shown in Table 1. We therefore conclude that, due to the type of the mutations in the binding pocket, our models show a hypsochromic shift in contrast to BR. This is a situation not unlike sRII, which also shows an "unusually" large hypsochromic shift with respect to BR,[26] although the retinal structures are very similar,[16,17] and the differences in the counterions contribute only a third of the spectral shift.[16] How this affects the isomerization pathway remains an unanswered question and should stimulate further studies.

The recently discovered MChR1 is the most red-shifted of the known ChRs.[6] While we did not consider MChR1 explicitly in this study, we may extend some conclusions from the study of the chlamydomonas-type ChRs to MChR1. First, two of the glutamates of the N-terminal region of the ChRs are replaced by neutral residues in MChR1 (in ChR1 numbering, E122 V and E136A). Since these glutamates are positioned in the loop and supposedly surrounded by solvent in our study, a replacement of them by neutral residues has no effect on the excitation energy,

which is confirmed by our perturbation analysis of the homology models. Residue E87 of ChR1 is replaced by a leucine in MChR1, which likely causes a bathochromic shift, as the comparison of the binding pocket models of ChR1 and ChR2 reveals (Table 2), E87 being absent in ChR2, too. Thus, the bathochromic shift of MChR1 with respect to the other ChRs may be explained by the lower number of negatively charged amino acids in the N-terminal region. Furthermore, several residues of the presumed binding pocket are exchanged to cause bathochromic shifts (e.g., V49K instead of V49S, D96A instead of D96H). However, since the homology of the MChR1 sequence to the other ChRs is lower than between any two of them,[6] a larger difference in the binding pocket composition occurs, a discussion of which is beyond the scope of the present study and certainly deserves future attention.

We modeled the color tuning in the ChRs based on multiple mutations on a BR template. A medium number of mutations in the binding pocket indeed leads to hypsochromic shifts of the excitation energy that are of the same order as the experimentally observed absorption maxima. The large hypsochromic shift can be traced back to two origins. While the effects of any given single mutation on the BR starting structure is small, the combination of multiple mutations in the binding pocket covers the majority of the hypsochromic shift. The other significant contribution is a stronger interaction of the retinal with its counterions, although the interaction mode is more flexible than in BR, switching between a direct interaction of the Schiff base with a counterion and a water molecule. If this switching actually leads to distinct conformations, that could explain the observed spectral pattern with multiple λ_{max},[5,9] remains a challenge for further studies. Moreover, it is yet to be clarified how the multiple conformations of the retinal (about 70% all-*trans* and 30% 13-*cis* and even small amounts of 9-*cis*) affect the absorption spectrum.[8]

Furthermore, the understanding of the binding pocket may be used to remove some of the uncertainties in homology models, especially regarding the orientation of the side chains, which is an ongoing endeavor in our group.

■ ASSOCIATED CONTENT

Supporting Information. The complete list of all single mutations and complete lists of authors for refs 39 and 55. This material is available free of charge via the Internet at http://pubs.acs.org.

■ AUTHOR INFORMATION

Corresponding Author

*E-mail: marcus.elstner@kit.edu. Phone: +49 (0)721/608-45705. Fax: +49 (0)721/608-45710.

■ ACKNOWLEDGMENT

This work was supported by the Deutsche Forschungsgemeinschaft (project FOR 1279, "Protein-based Photoswitches" as optogenetic tools). H. W. gratefully acknowledges a research fellowship from the Japan Society for the Promotion of Science.

■ REFERENCES

(1) Nagel, G.; Ollig, D.; Fuhrmann, M.; Kateriya, S.; Musti, A. M.; Bamberg, E.; Hegemann, P. *Science* **2002**, *296*, 2395–2398.

(2) Nagel, G.; Szellas, T.; Huhn, W.; Kateriya, S.; Adeishvili, N.; Berthold, P.; Ollig, D.; Hegemann, P.; Bamberg, E. *Proc. Natl. Acad. Sci. U.S.A.* **2003**, *100*, 13940–13945.

(3) Ernst, O. P.; Sánchez Murcia, P. A.; Daldrop, P.; Tsunoda, S. P.; Kateriya, S.; Hegemann, P. *J. Biol. Chem.* **2008**, *283*, 1637–1643.

(4) Zhang, F.; Prigge, M.; Beryière, F.; Tsunoda, S. P.; Mattis, J.; Yizhar, O.; Hegemann, P.; Deisseroth, K. *Nat. Neurosci.* **2008**, *11*, 631–633.

(5) Kianianmomeni, A.; Stehfest, K.; Nematollahi, G.; Hegemann, P.; Hallmann, A. *Plant Physiol.* **2009**, *151*, 347–366.

(6) Govorunova, E. G.; Spudich, E. N.; Lane, C. E.; Sineshchekov, O. A.; Spudich, J. L. *mBio* **2011**, *2*, e00115–11.

(7) Stehfest, K.; Hegemann, P. *ChemPhysChem* **2010**, *11*, 1120–1126.

(8) Nack, M.; Radu, I.; Bamann, C.; Bamberg, E.; Heberle, J. *FEBS Lett.* **2009**, *583*, 3676–3680.

(9) Ritter, E.; Stehfest, K.; Berndt, A.; Hegemann, P.; Bartl, F. J. *J. Biol. Chem.* **2008**, *283*, 35033–35041.

(10) Radu, I.; Bamann, C.; Nack, M.; Nagel, G.; Bamberg, E. *J. Am. Chem. Soc.* **2009**, *131*, 7313–7319.

(11) Boyden, E. S.; Zhang, F.; Bamberg, E.; Nagel, G.; Deisseroth, K. *Nat. Neurosci.* **2005**, *8*, 1263–1268.

(12) Deisseroth, K. *Nat. Methods* **2011**, *8*, 26–29.

(13) Birge, R. R.; Zhang, C.-F. *J. Chem. Phys.* **1990**, *92*, 7178–7195.

(14) Berthold, P.; Tsunoda, S. P.; Ernst, O. P.; Mages, W.; Gradmann, D.; Hegemann, P. *Plant Cell* **2008**, *20*, 1665–1677.

(15) Hegemann, P.; Möglich, A. *Nat. Methods* **2011**, *8*, 39–42.

(16) Hoffmann, M.; Wanko, M.; Strodel, P.; König, P. H.; Frauenheim, T.; Schulten, K.; Thiel, W.; Tajkhorshid, E.; Elstner, M. *J. Am. Chem. Soc.* **2006**, *128*, 10808–10818.

(17) Hayashi, S.; Tajkhorshid, E.; Pebay-Peyroula, E.; Royant, A.; Landau, E. M.; Navarro, J.; Schulten, K. *J. Phys. Chem. B* **2001**, *105*, 10124–10131.

(18) Tomasello, G.; Olaso-González, G.; Altoè, P.; Stenta, M.; Serrano-Andrés, L.; Merchán, M.; Orlandi, G.; Bottoni, A.; Garavelli, M. *J. Am. Chem. Soc.* **2009**, *131*, 5172–5186.

(19) Altun, A.; Yokoyama, S.; Morokuma, K. *J. Phys. Chem. B* **2008**, *112*, 6814–6827.

(20) Altun, A.; Yokoyama, S.; Morokuma, K. *J. Phys. Chem. A* **2009**, *113*, 11685–11692.

(21) Fujimoto, K.; Hasegawa, J.-Y.; Nakatsuji, H. *Bull. Chem. Soc. Jpn.* **2009**, *82*, 1140–1148.

(22) Fujimoto, K.; Hasegawa, J.-Y.; Hayashi, S.; Kato, S.; Nakatsuji, H. *Chem. Phys. Lett.* **2005**, *414*, 239–242.

(23) Sekharan, S.; Sugihara, M.; Buss, V. *Angew. Chem. Intl. Ed.* **2007**, *46*, 269–271.

(24) Trabanino, R. J.; Veidehi, N.; Goddard, W. A., III. *J. Phys. Chem. B* **2006**, *110*, 17230–17239.

(25) Hufen, J.; Sugihara, M.; Buss, V. *J. Phys. Chem. B* **2004**, *108*, 20419–20426.

(26) Altoè, P.; Cembran, A.; Olivucci, M.; Garavelli, M. *Proc. Natl. Acad. Sci. U.S.A.* **2010**, *107*, 20172–20177.

(27) Wanko, M.; Hoffmann, M.; Strodel, P.; Koslowski, A.; Thiel, W.; Neese, F.; Frauenheim, T.; Elstner, M. *J. Phys. Chem. B* **2005**, *109*, 3606–3615.

(28) Frähmcke, J. S.; Wanko, M.; Phatak, P.; Mroginski, M. A.; Elstner, M. *J. Phys. Chem. B* **2010**, *114*, 11338–11352.

(29) Luecke, H.; Schobert, B.; Richter, H.-T.; Cartailler, J.-P.; Lanyi, J. K. *J. Mol. Biol.* **1999**, *291*, 899–911.

(30) Brooks, B. R.; Bruccoleri, R. E.; Olafson, B. D.; States, D. J.; Swaminathan, S.; Karplus, M. *J. Comput. Chem.* **1983**, *4*, 187–217.

(31) Sasaki, J.; Lanyi, J. K.; Needleman, R.; Yoshizawa, T.; Maeda, A. *Biochemistry* **1994**, *33*, 3178–3184.

(32) Brown, L. S.; Sasaki, J.; Kandori, H.; Maeda, A.; Needleman, R.; Lanyi, J. K. *J. Biol. Chem.* **1995**, *270*, 27122–27126.

(33) Dinner, A. R.; Lopez, X.; Karplus, M. *Theor. Chem. Acc.* **2003**, *109*, 118–124.

(34) Cui, Q.; Elstner, M.; Kaxiras, E.; Frauenheim, T.; Karplus, M. *J. Phys. Chem. B* **2001**, *105*, 569–585.

(35) Elstner, M.; Cui, Q. Combined QM/MM methods for the simulation of condensed phase processes using an approximate DFT approach. In *Solvation Effects. Methods and Applications*; Canuto, S., Ed.; Challenges and Advances in Computational Chemistry and Physics 6; Springer: Dordrecht, The Netherlands, 2008; pp 381−405.
(36) Cui, Q.; Elstner, M. Multi-scale QM/MM methods with Self-Consistent-Charge Density-Functional Tight-Binding (SCC-DFTB). In *Multi-scale Quantum Models for Biocatalysis*; Lee, T.-S., York, D., M., Eds.; Challenges and Advances in Computational Chemistry and Physics 7; Springer: Dordrecht, The Netherlands, 2009; pp 173−196.
(37) Elstner, M.; Porezag, D.; Jungnickel, G.; Elsner, J.; Haugk, M.; Frauenheim, T.; Suhai, S.; Seifert, G. *Phys. Rev. B* **1998**, *58*, 7260–7268.
(38) Zhou, H.; Tajkhorshid, E.; Frauenheim, T.; Suhai, S.; Elstner, M. *Chem. Phys.* **2002**, *277*, 91–103.
(39) MacKerell, A. D., Jr.; Bashford, D.; Bellott, M.; Dunbrack, R. L., Jr.; Evanseck, J. D.; Field, M. J.; Fischer, S.; Gao, J.; Guo, H.; Ha, S.; et al. *J. Phys. Chem. B* **1998**, *102*, 3586–3616.
(40) Yang, Y.; Yu, H.; York, D.; Cui, Q.; Elstner, M. *J. Phys. Chem. A* **2007**, *111*, 10861–10873.
(41) König, P. H.; Hoffmann, M.; Frauenheim, T.; Cui, Q. *J. Phys. Chem. B* **2005**, *109*, 9082–9095.
(42) Nosé, S. *J. Chem. Phys.* **1984**, *81*, 511–519.
(43) Hoover, W. G. *Phys. Rev. A* **1985**, *31*, 1695–1697.
(44) Weber, W.; Thiel, W. *Theor. Chem. Acc.* **2000**, *103*, 495–506.
(45) Koslowski, A.; Beck, M.; Thiel, W. *J. Comput. Chem.* **2003**, *24*, 714–726.
(46) Thiel, W. *MNDO99, version 6.1*; Max-Planck-Institut für Kohlenforschung: Mülheim an der Ruhr, Germany, 2004.
(47) Neese, F. *J. Chem. Phys.* **2003**, *119*, 9428–9443.
(48) Neese, F. *ORCA—An ab initio, density functional and semiempirical program package*, version 2.4, revision 41; Max Planck Institut für Strahlenchemie: Mülheim an der Ruhr, Germany, 2005.
(49) Schäfer, A.; Horn, H.; Ahlrichs, R. *J. Chem. Phys.* **1992**, *97*, 2571–2577.
(50) As one-electron basis for the SORCI calculation, averaged approximate natural orbitals were used, resulting from a MRDDCI3 calculation (multireferential, difference dedicated configuration interaction with 3 degrees of freedom) with a CAS(4,4) reference space after the initial restricted Hartree−Fock calculation and generation of improved virtual orbitals.
(51) Wanko, M.; Hoffmann, M.; Frauenheim, T.; Elstner, M. *J. Phys. Chem. B* **2008**, *112*, 11462–11467.
(52) Wanko, M.; Hoffmann, M.; Frähmcke, J. S.; Frauenheim, T.; Elstner, M. *J. Phys. Chem. B* **2008**, *112*, 11468–11478.
(53) Phatak, P.; Frähmcke, J. S.; Wanko, M.; Hoffmann, M.; Strodel, P.; Smith, J. C.; Suhai, S.; Bondar, A. N.; Elstner, M. *J. Am. Chem. Soc.* **2009**, *131*, 7064–7078.
(54) Sineshchekov, O. A.; Jung, K.-H.; Spudich, J. L. *Proc. Natl. Acad. Sci. U.S.A.* **2002**, *99*, 8689–8694.
(55) Suzuki, T.; Yamasaki, K.; Fujita, S.; Oda, K.; Iseki, M.; Yoshida, K.; Watanabe, M.; Daiyasu, H.; Toh, H.; Asamizu, E.; et al. *Biochem. Biophys. Res. Comun.* **2003**, *301*, 711–717.
(56) First letter and number refers to BR sequence, and last letter is corresponding residue in the ChRs.
(57) Tsunoda, S. P.; Hegemann, P. *Photochem. Photobiol.* **2009**, *85*, 564–569.
(58) Guex, N.; Peitsch, M. C. *Electrophoresis* **1997**, *18*, 2714–2723.
(59) Schwede, T.; Kopp, J.; Guex, N.; Peitsch, M. C. *Nucleic Acids Res.* **2003**, *31*, 3381–3385.
(60) Nack, M.; Radu, I.; Gossing, M.; Bamann, C.; Bamberg, E.; von Mollard, G. F.; Heberle, J. *Photochem. Photobiol. Sci.* **2010**, *9*, 194–198.
(61) Rajput, J.; Rahbek, D. B.; Andersen, L. H.; Hirshfeld, A.; Sheves, M.; Altoè, P.; Orlandi, G.; Garavelli, M. *Angew. Chem. Intl. Ed.* **2010**, *49*, 1790–1793.